

The Size–Mass Relation of Post-Starburst Galaxies in the Local Universe

XINKAI CHEN ^{1,2} ZESEN LIN ^{1,2} XU KONG ^{1,2,3} ZHIXIONG LIANG,^{1,2} GUANGWEN CHEN,^{1,2} AND HONG-XIN ZHANG^{1,2}

¹*CAS Key Laboratory for Research in Galaxies and Cosmology, Department of Astronomy, University of Science and Technology of China, Hefei 230026, China*

²*School of Astronomy and Space Sciences, University of Science and Technology of China, Hefei 230026, China*

³*Frontiers Science Center for Planetary Exploration and Emerging Technologies, University of Science and Technology of China, Hefei, Anhui, 230026, China*

ABSTRACT

We present a study of the size–mass relation for local post-starburst (PSB) galaxies at $z \lesssim 0.33$ selected from the Sloan Digital Sky Survey Data Release 8. We find that PSB galaxies with stellar mass (M_*) at $10^9 M_\odot < M_* < 10^{12} M_\odot$ have their galaxy size smaller than or comparable with those of quiescent galaxies (QGs). After controlling redshift and stellar mass, the sizes of PSBs are $\sim 13\%$ smaller on average than those of QGs, such differences become larger and significant towards the low- M_* end, especially at $10^{9.5} M_\odot \lesssim M_* \lesssim 10^{10.5} M_\odot$ where PSBs can be on average $\sim 19\%$ smaller than QGs. In comparison with predictions of possible PSB evolutionary pathways from cosmological simulations, we suggest that a fast quenching of star formation following a short-lived starburst event (might be induced by major merger) should be the dominated pathway of our PSB sample. Furthermore, by cross-matching with group catalogs, we confirm that local PSBs at $M_* \lesssim 10^{10} M_\odot$ are more clustered than more massive ones. PSBs resided in groups are found to be slightly larger in galaxy size and more disk-like compared to field PSBs, which is qualitatively consistent with and thus hints the environment-driven fast quenching pathway for group PSBs. Taken together, our results support multiple evolutionary pathways for local PSB galaxies: while massive PSBs are thought of as products of fast quenching following a major merger-induced starburst, environment-induced fast quenching should play a role in the evolution of less massive PSBs, especially at $M_* \lesssim 10^{10} M_\odot$.

Keywords: galaxy evolution (594); galaxy structure (622); galaxy quenching (2040); post-starburst galaxies (2176);

1. INTRODUCTION

Galaxies in the local Universe show a clear bimodality in the color–magnitude diagram (Baldry et al. 2004), which suggests that they can be naturally separated into two populations: star-forming galaxies (SFGs) in the “blue cloud” and quiescent galaxies (QGs) in the “red sequence”. The dearth of galaxies in the transitional region, which is known as “green valley” (GV) region (Martin et al. 2007; Salim et al. 2007; Schiminovich et al. 2007; Wyder et al. 2007; Salim 2014), indicates that the migration from blue cloud to red sequence is relatively rapid (Martin et al. 2007). Therefore, investigations of intermediate galaxies resided in this transitional region

can give insights into galaxy evolution (e.g., Schawinski et al. 2014; Gu et al. 2018; Suess et al. 2021; Lin et al. 2022).

Post-starburst (PSB) galaxies, also known as E+A/K+A galaxies, have spectral features of elliptical galaxies and A-type stars (Dressler & Gunn 1983; Poggianti et al. 1999). These galaxies are observed to reside in the GV region (e.g., Wong et al. 2012; Greene et al. 2021), implying that they might be one kind of transitional galaxies. The strong Balmer absorption lines indicate that those galaxies have experienced starbursts within the last 1 Gyr since the lifetime of an A-type star is about 1 Gyr. But they show no sign of ongoing star formation as first indicated by the non-detection of the [O II] emission lines (Goto 2005).

As one of the fundamental scaling relations, galaxy size–stellar mass (M_*) relation and its evolution with

cosmic time are widely used to probe the assembly history of galaxies and thus study galaxy evolution (e.g., Williams et al. 2010; Newman et al. 2012; van der Wel et al. 2014; Shibuya et al. 2015; Kawinwanichakij et al. 2021). When $M_* \lesssim 10^{11} M_\odot$, galaxy sizes of SFGs are found to be larger than those of QGs at a fixed M_* (Shen et al. 2003; van der Wel et al. 2014; Kawinwanichakij et al. 2021), while GV galaxies tend to have galaxy sizes in between (Salim 2014; Gu et al. 2018; Suess et al. 2021).

As for PSB galaxies, high-redshift samples were found to have smaller sizes compared to QGs at a fixed M_* (Whitaker et al. 2012; Yano et al. 2016). Particularly, Almaini et al. (2017) studied PSB galaxies at high redshift ($z > 1$) and found that the sizes of PSB galaxies is smaller than that of QGs, they claimed that massive passive galaxies are formed from proto-spheroids, then rapid quenching creates red nuggets with post-starburst features, and finally the gradual growth in size causes the sizes increase. In this physical picture, galaxies may experience violent events, such as galaxy mergers. The process period can be less than a few hundred Myr, and the intense star formation quickly exhaust gas and build a dense center core. As new stars are formed in the center, fast process can significantly change galaxies structure, causing a few times smaller size in comparison with their progenitor (Hopkins et al. 2013; Wellons et al. 2015; Wu et al. 2018).

However, this evolutionary pathway might be not true for PSB galaxies at all redshifts. On the one hand, based on ultra-deep optical spectra of PSBs at $z \sim 0.8$, studies combining stellar populations and galaxy structure supported a fast quenching pathway associated with centrally concentrated starbursts and thus dramatic structural changes for PSBs at this epoch (Wu et al. 2018, 2020; D'Eugenio et al. 2020). On the other hand, Maltby et al. (2018) presented a comparison between lower redshift ($0.5 < z < 1$) and higher redshift ($z > 1$) PSB galaxies, in which the authors found that lower redshift PSBs are less concentrated than their high-redshift analogues, suggesting that the processes that are responsible for PSB evolution at intermediate-redshift might be less violent and there may have different quenching routes at different redshifts.

For local PSB galaxies, one might wonder whether the galaxy size–mass relation observed for intermediate- and high-redshift PSBs (i.e., smaller galaxy sizes compared to QGs at a fixed M_*) is still applicable, and thus share the same fast quenching picture used to explain the compact morphology of high-redshift PSBs. Observational studies highlighted the diversity of this population and claimed different M_* -dependent evolutionary

pathways of PSBs including the fast quenching with significant structural changes and cyclic evolution of SFGs or QGs without substantial morphological transformation (Pawlik et al. 2018). These pathways were also reproduced by cosmological simulations (Pawlik et al. 2019). Recent surveys of PSB galaxies in local galaxy groups/clusters further reported a positive correlation between the incidence of PSB galaxies and environment indicators, which is suggestive of a nonnegligible effect of environment in the evolution of PSB galaxies (Poggianti et al. 2017; Paccagnella et al. 2019).

Given that structural changes are closely related with the various evolutionary pathways of PSB galaxies in the local Universe (Pawlik et al. 2018, 2019), the size–mass relation could be an important probe to clarify the evolution of PSBs and, however, is still lacking in direct study. Therefore, we present a study of the size–mass relation for local PSB galaxies based on data from the Sloan Digital Sky Survey Data Release 8 (SDSS DR8; Aihara et al. 2011). This paper is organized as follows. In Section 2 we describe our sample. The main result is presented and studied in Section 3. We discuss the implication of our findings in Section 4 and summarize in Section 5. Throughout this paper, we adopt a Λ CDM cosmology with $\Omega_m = 0.3$, $\Omega_\Lambda = 0.7$ and $H_0 = 70 \text{ km s}^{-1} \text{ Mpc}^{-1}$.

2. SAMPLE SELECTION

2.1. *Post-starburst Galaxies*

PSB galaxies are defined by two criteria, one is significant recent star formation, which is indicated by the presence of a large population of short lifetime ($< 1 \text{ Gyr}$) A type stars and thus the observable strong Balmer absorption, the other one is no ongoing star formation, which is traced by weak emission lines (e.g., H α and/or [O II]). However, the use of nebular emission lines to select PSBs may bias the selection against galaxies hosting narrow-line active galactic nuclei or shocks and also exclude galaxies that are PSBs but not fully quenched (Yan et al. 2006; Wild et al. 2007, 2009; Yesuf et al. 2014). On the other hand, not selecting on emission lines may cause some PSBs to be indistinguishable from star-forming population (Wild et al. 2007).

Here, we select PSB galaxies based on the MPA-JHU catalog¹ for the SDSS DR8 galaxy spectra, adopting the criteria of $H\delta_A > 4 \text{ \AA}$, $EW(H\alpha) < 3 \text{ \AA}$, and the median spectral signal-to-noise ratio per pixel of $S/N > 5$. After careful visual inspection of the selected spectra, we further require spectra to meet $H\delta_A/\sigma(H\delta_A) > 3$ and

¹ http://www.sdss3.org/dr10/spectro/galaxy_mpa_jhu.php

$\chi_{\text{red,H}\alpha}^2 > 0$ to ensure reliable measurements of $\text{H}\delta_{\text{A}}$ and $\text{EW}(\text{H}\alpha)$, respectively.² 22 sources with non-zero SDSS “zWarning” bitmask³ (i.e., the best-fit classification or redshift might be not reliable) are also examined via spectra, optical images, and cross-matched information in other online database (e.g., SIMBAD; Wenger et al. 2000), 17 of them are identified as QSOs or white dwarfs and are removed from the sample. Relaxing these criteria to include a larger region on the $\text{EW}(\text{H}\alpha)$ – $\text{H}\delta_{\text{A}}$ plane (e.g., Chen et al. 2019) or applying a stricter cut on $\text{H}\delta_{\text{A}}$ (e.g., Goto 2007) would not change our main results significantly.

To obtain reliable size measurements, we match the sample with the UPenn SDSS PhotDec Catalog (Meert et al. 2015, 2016; see Section 2.2), which naturally introduces a r band magnitude limit of $14.0 \text{ mag} < r < 17.77 \text{ mag}$ (Meert et al. 2015). We also require galaxies to have stellar mass (M_* ; see Section 2.2) between 10^9 to $10^{12} M_{\odot}$ within which most of the selected PSBs locate. After these criteria, we obtain 1,479 candidates of PSB galaxies. These PSB galaxies have a redshift ranged from 0.012 to 0.324 and with a median and 1- σ range of $0.130^{+0.069}_{-0.061}$.

2.2. Determination of Physical Properties

The UPenn SDSS PhotDec Catalog provides point spread function (PSF)-corrected 2D profile fitting results for $\sim 7 \times 10^5$ galaxies using a variety of models, including de Vaucouleurs, Sérsic, de Vaucouleurs+Exponential, and Sérsic+Exponential models. The fitting pipeline is called PyMorph (Vikram et al. 2010), which is a python based automated software pipeline built on SExtractor (Bertin & Arnouts 1996) and the 2D fitting routine GALFIT (Peng et al. 2002). To be consistent with previous PSB studies (e.g., Yano et al. 2016; Almaini et al. 2017; Wu et al. 2018, 2020) and enable plausible comparisons in the following analyses, we adopt the effective radius (R_e) measured along the semi-major axis derived from the single Sérsic model fitting in r -band as our fiducial galaxy size measurement. This choice of R_e is generally consistent with most of PSB literature we used for comparison in terms of both the derivation method and the sampled rest-frame wavelengths (see Section 4.5 for more details). The statistical uncertainties of size measurements of our PSB sample have a median value and 1- σ range of $3.5^{+4.1}_{-1.9}\%$. While the systematic uncertainties, together with the PSF ef-

fects, of the size measurement will be discussed in Section 4.5.

The total stellar mass is taken from the MPA-JHU catalog, which is the median value of the probability distribution function (PDF) of the total M_* constructed from the *ugriz* galaxy photometry and a large library of spectral energy distribution (SED) models sampled the full plausible ranges of galaxy physical properties (Kauffmann et al. 2003). To generate model SEDs, a Kroupa (2001) initial mass function, a Charlot & Fall (2000) dust attenuation curve, and the Bruzual & Charlot (2003) population synthesis code are adopted, while star formation history is assumed to be an exponentially declining continuous star formation superimposed with random bursts. The PDF of each galaxy parameter (e.g., M_*) is computed via weighting each model by the corresponding $\exp(-\chi^2/2)$ and then binning them as a function of the parameter value. More detailed descriptions can be found in Kauffmann et al. (2003) or Salim et al. (2007).

The measurements of star formation rate (SFR) are also taken from the MPA-JHU catalog, which are the median values of the total SFR PDFs. For SFGs with strong emission lines, SFRs within the SDSS fiber aperture are estimated from emission lines as described in Brinchmann et al. (2004), while the ones beyond the fiber are computed from the galaxy photometry, namely the similar photometric method used to derived M_* described above, but ultraviolet photometry is involved to constrain SFR. For galaxies with weak emission lines (e.g., our PSB sample), SFRs are estimated via the photometric method using the integrated ultraviolet/optical photometry. We refer the reader to Salim et al. (2007) for a detailed introduction.

2.3. Star-forming and Quiescent Galaxies

To compare PSB galaxies with SFGs and QGs, we follow Woo et al. (2013) to divide galaxies into star-forming and quiescent galaxies based on the divided line of $\log \text{SFR}(M_{\odot} \text{ yr}^{-1}) = 0.64 \times \log M_*(M_{\odot}) - 7.22$. 313,427 SFGs and 327,700 QGs are selected and defined as Sample SFG and Sample QG, respectively. The distributions of SFGs, QGs, and PSBs on the M_* –SFR diagram are shown in Figure 1. The red solid line is the divided line from Woo et al. (2013), which clearly indicates the division between SFGs and QGs in our sample. It is not surprising that most of the PSBs are located near the divided line with a relatively large scatter, because this population is mainly known as galaxies in a transition phase of galaxy evolution for which the specific pathway, however, is still in debate (Pawlik et al. 2018, 2019).

² Here, $\sigma(\text{H}\delta_{\text{A}})$ is the uncertainty of index $\text{H}\delta_{\text{A}}$, while $\chi_{\text{red,H}\alpha}^2$ is the reduced chi-squared of the emission line fitting of $\text{H}\alpha$.

³ <https://www.sdss.org/dr16/algorithms/bitmasks/#ZWARNING>

2.4. Control Sample

As the sample size of Sample PSB is much smaller than that of Sample SFG or QG, we generate two control samples to better compare the relation between SFGs, QGs, and PSB galaxies. We take Sample SFG or QG as a parent sample and create control sample with similar redshift and stellar mass. For each galaxy in Sample PSB, we search its nearest neighbors in the Sample SFG (or Sample QG) on the M_*-z plane within a distance of 0.03 dex in $\log M_*(M_\odot)$ and 0.005 in z . Each galaxy in the parent samples only enters the control sample once. If less than three galaxies are matched, we expand the $\Delta \log M_*(M_\odot)$ and Δz tolerances by 0.01 dex and 0.001, respectively. 95.3% of PSB galaxies can obtain sufficient matches in the first search. In the end, each galaxy in Sample PSB has three matched SFGs and QGs with similar M_* and redshift. Thus, the resulting Sample Control SFG and Sample Control QG both have a sample size of 4,437.

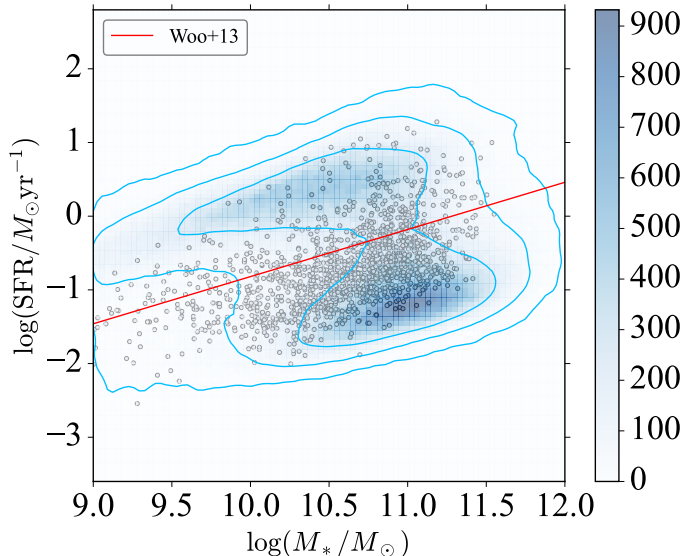


Figure 1. SFR versus M_* for our selected PSB candidates. The grey points indicate the distribution of individual PSBs. The color map shows the number density of all galaxies used in this work (e.g., Samples SFG, PSB, and QG), while the contours encompass 99.7%, 95.5%, and 68.3% of them, respectively. The red solid line is the divided line for SFGs and QGs following Woo et al. (2013).

3. RESULTS

3.1. The M_* Distribution of PSBs

Firstly, we show the stellar mass distribution of PSB galaxies in Figure 2. Clearly, QGs tend to be more massive compared to the other two samples, while the median of $\log(M_*/M_\odot)$ are 10.93, 10.66, and 10.47 for QGs,

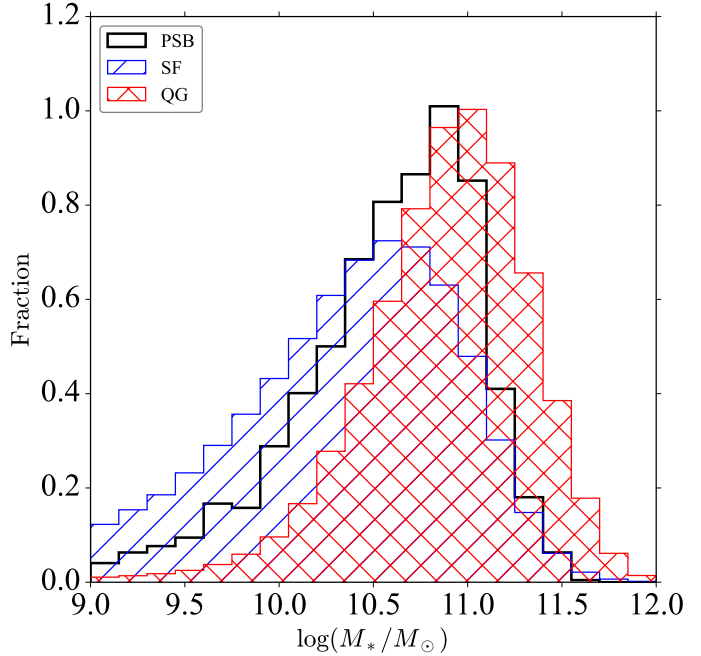


Figure 2. The distribution of stellar mass for Samples PSB (black), SFG (blue), and QG (red).

PSBs, and SFGs, respectively. Maltby et al. (2018) reported a strong redshift evolution of the M_* distribution for their photometrically selected PSB sample (i.e., $M_* \lesssim 10^{10} M_\odot$ for most of their PSBs at $0.5 < z < 1$ and $M_* \gtrsim 10^{10} M_\odot$ for those at $1 < z < 2$), suggesting less massive PSB galaxies in lower-redshift Universe. However, the majority (88.8%) of our local PSBs have M_* greater than $10^{10} M_\odot$. Such apparent conflict is due to the fact that our samples are selected from the MPA-JHU catalog released in the SDSS DR8, within which most of galaxies are from a flux-limited sample. The main galaxy spectroscopic survey of SDSS contributes most of galaxies in the MPA-JHU catalogs⁴ and is sampled to a r -band magnitude limit of 17.77 mag (Strauss et al. 2002), corresponding to a stellar mass of $M_* \gtrsim 2 \times 10^{10} M_\odot$ at the median redshift of Sample PSB ($z = 0.13$) for a typical color of green valley galaxies (e.g., Schawinski et al. 2014) based on the Bell et al. (2003) calibration. In other words, our PSB sample is naturally biased toward the massive end of low-redshift PSB galaxies, although less massive PSBs (i.e., $M_* \lesssim 10^{10} M_\odot$) are expected to be predominant in this population (Wild et al. 2016; Maltby et al. 2018).

As the sample size of PSBs is small, we are unable to construct a mass complete sample to remove any poten-

⁴ <https://wwwmpa.mpa-garching.mpg.de/SDSS/DR7/Data/allldr72spectro-mpajhu.par>

tial bias arising from sample selection when comparing with SFGs and QGs. Instead, we will use control samples described in Section 2.4 in the following analysis to avoid this problem.

3.2. Size-Mass Relation

In this section, we show the typical size-mass relation for SFGs, QGs, and PSB galaxies. In the left panel of Figure 3, we present the overall distributions of Samples SFG, QG, and PSB on the stellar size-mass diagram. To parameterize their overall trends, we follow van der Wel et al. (2014) and fit the distributions with a formula of $R_e/\text{kpc} = A \times m_*^\alpha$ ($m_* \equiv M_*/7 \times 10^{10} M_\odot$) in the M_* ranges of $10^9 M_\odot < M_* < 10^{12} M_\odot$ and $10^{10} M_\odot < M_* < 10^{12} M_\odot$ for SFGs and QGs, respectively. The best-fit results are also plotted in Figure 3.

Although the PSB galaxies span a relatively large range in size at a fixed M_* , the number density contour of this population exhibits a large overlap with that of QGs and is only slightly lower than the best-fit size-mass relation of QGs, suggesting a very similar size-mass relation between these two populations. On the other hand, the sizes of PSBs are much smaller than those of SFGs at a fixed M_* , while the differences become larger towards the low-mass end.

In order to clearly exhibit the difference in the size-mass relation between Samples PSB and QG, we calculate the running medians for the three samples at $10^9 M_\odot < M_* < 10^{12} M_\odot$, which are shown in the right panel of Figure 3. Only bins with more than 10 galaxies are considered and plotted. The $1-\sigma$ uncertainties of the running medians are also computed via the bootstrapping method and denoted as shadow regions in the figure. The median size-mass relations of Samples SFG and QG have a cross at the most massive end (i.e., $M_* \sim 10^{11.0} M_\odot$), which is consistent with the finding in low-redshift Universe based on either deep field (e.g., van der Wel et al. 2014; Mowla et al. 2019) or wide field (e.g., Mosleh et al. 2013; Roy et al. 2018) surveys. Obviously, SFGs are found to have the largest galaxy size in most of the M_* bins. As indicated by the relative position between the contours of PSBs and the best-fit size-mass relation of QGs, the median sizes of PSBs are smaller than those of QGs, suggesting that PSBs seem to be more compact than QGs. This result is further examined using the control samples in Section 3.3 since we have demonstrated that Sample PSB is not mass complete (see Section 3.1).

3.3. Comparison with Control Samples

As mentioned earlier, we attempt to utilize the control samples to remove any potential bias due to the incompleteness of sample construction. Here, we show the

size-mass relation in the M_* range of $10^9 M_\odot < M_* < 10^{12} M_\odot$ for Sample PSB, Control SFG, and Control QG in Figure 4. The running medians of galaxy size of these samples and the corresponding uncertainties via the bootstrapping method are calculated.

Comparing with the best-fit size-mass relation of Sample QG, although the median relation of Control QG shows a small decrease at $M_* \gtrsim 10^{10.5} M_\odot$, the median galaxy sizes of PSBs are still smaller than those of QGs in most of the M_* we explored. Such differences between PSBs and QGs become more significant towards the low-mass end. Thus we conclude that PSBs tend to have a more compact morphology compared to Control QG at $M_* \lesssim 10^{11.0} M_\odot$. On the other hand, the median size-mass relation of Control SFG only has small variations around the median relation of its parent sample, leading to a much larger galaxy size of SFG population than that of Sample PSB after controlling redshift and M_* . At $M_* \sim 10^{11.5} M_\odot$, the median size-mass relations of the three populations are consistent with each other within the uncertainties.

We summarize the median values of R_e and the corresponding $1-\sigma$ uncertainties in bins of M_* for Sample PSB, Control SFG, and Control QG, together with the numbers of galaxies within each bin (N), in Table 1. To quantify the strength of the differences, we perform Kolmogorov-Smirnov (KS) tests for the differences in R_e between Sample PSB and other two control samples. A KS test p -value of 0.05 means that there is 95 per cent confidence that we can reject the null hypothesis that the two samples are drawn from the same distribution. The one-by-one R_e differences in bins of M_* and the resulting p -values from KS tests are shown in Table 2. The galaxy sizes of PSBs are estimated to be on average $\sim 13\%$ smaller than those of QGs, especially at $10^{9.5} M_\odot \lesssim M_* \lesssim 10^{10.5} M_\odot$ where PSBs can be on average $\sim 19\%$ smaller than QGs. Obviously, the size differences between QGs and PSBs are significant at $10^{9.6} M_\odot \lesssim M_* \lesssim 10^{11.1} M_\odot$, with all the p -values below 0.05.

As shown in Figure 1, the distribution of PSB galaxies in the M_* -SFR plane biases toward the QG side. One might wonder whether this distribution bias has any effect on the size distribution of PSBs. Observationally, PSBs in the color-mass (or magnitude) plane tend to reside in the GV region (e.g., Wong et al. 2012; Greene et al. 2021), within which galaxies are believed to be in a transitional phase and have larger size compared to QGs (Salim 2014; Gu et al. 2018; Suess et al. 2021). Therefore, we would not expect that the distribution bias in M_* -SFR plane has any contribution to the compact morphology of PSBs. However, to totally

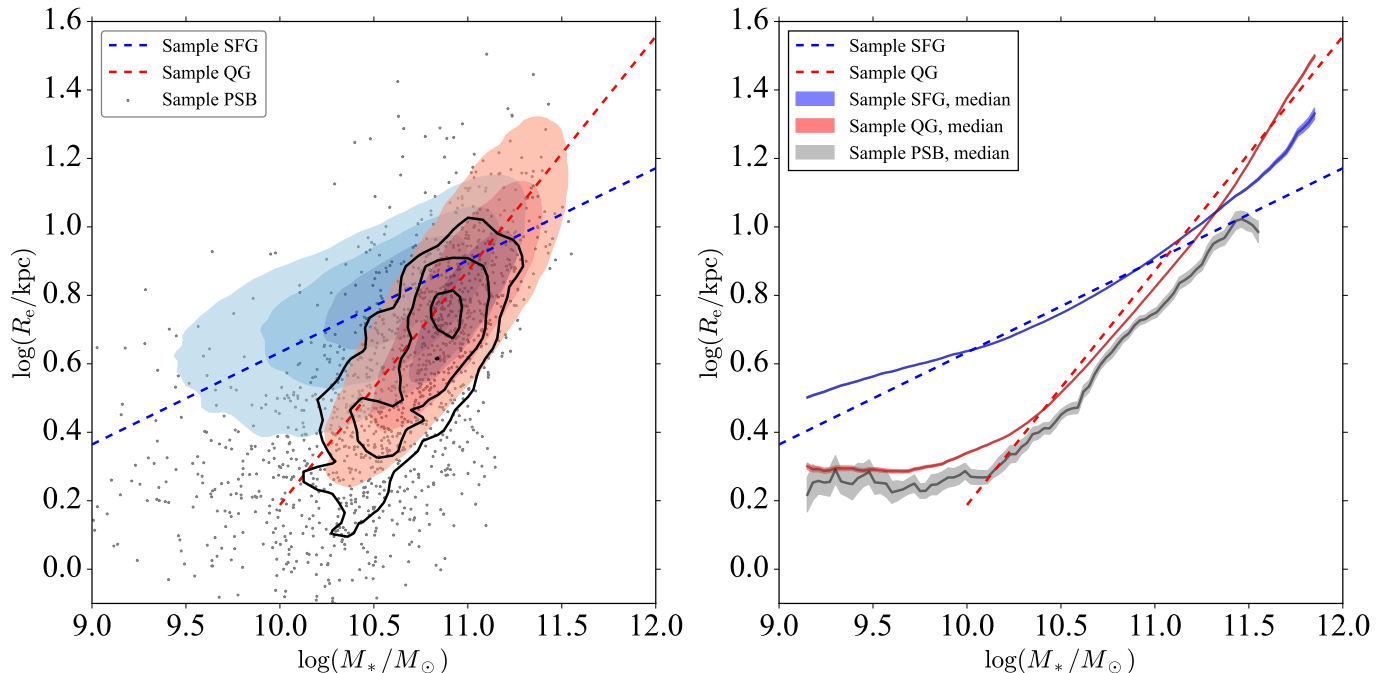


Figure 3. Size–mass relation for our samples. Left: the overall distributions of SFGs (blue filled contours), QGs (red filled contours), and PSBs (black open contours) on the size–mass diagram. The contours enclose 25%, 50%, and 75% of the corresponding samples, respectively. The blue (red) dashed line is the best-fit for the size–mass relation in formula of $R_e/\text{kpc} = A \times m_*^\alpha$ ($m_* \equiv M_*/7 \times 10^{10} M_\odot$; van der Wel et al. 2014) for SFGs (QGs). The grey points exhibit the distribution of individual PSBs. Right: the running median of galaxy size as a function of M_* for Samples SFG (blue), QG (red), and PSB (grey). The solid curves represent the running median values, while the shadow regions denote the corresponding $1-\sigma$ uncertainties. Only bins with more than 10 galaxies are plotted. The dashed lines are the same as those in the left panel.

unveil the role of this bias, we further construct a three-parameter control sample using the method described in Section 2.4 but control SFR at the same time (i.e., a M_* –SFR– z control sample, defined as Sample Control SFR hereafter). The median size–mass relation for this new control sample is given in Table 1 and denoted by green curve in Figure 4, together with its $1-\sigma$ uncertainty.

As expected, Sample Control SFR has an intermediate galaxy size between SFGs and QGs, which is significantly larger than that of Sample PSB. Namely, the removal of the distribution bias in the M_* –SFR plane, on the contrary, reinforces the result of an extreme compact morphology for PSBs described earlier.

In the bottom panel of Figure 4, we show the differences of the running medians between Sample PSB and the control samples. The results from the top panel are more obvious in this plot. In short, the sizes of PSBs are smaller compared to QGs after controlling M_* and redshift, and the differences between them become larger and significant towards the low-mass end.

3.4. Differences in Concentration and Sérsic Index

Besides the effective radius R_e , the more compact morphology of PSB galaxies compared to QGs also can be traced by the concentration C or the best-fit Sérsic index n . We show the comparisons of the concentration between Sample PSB and three control samples in Figure 5. Here, the concentration is defined as $C = R_{90,r}/R_{50,r}$ (Graham et al. 2005), where $R_{50,r}$ and $R_{90,r}$ are radii containing 50% and 90% of the Petrosian fluxes in r -band, respectively. Choosing the concentration defined by Petrosian fluxes (rather than the ones from the single Sérsic fit where our adopted R_e is derived) ensures an independent verification of our results.

It is clear that PSBs have the largest C at $M_* \lesssim 10^{11.0} M_\odot$ compared to all of the three control samples. The differences in C in bins of M_* are also given in Table 2, together with the corresponding p -values of KS tests. The concentrations of PSBs are found to be larger than those of Control QGs by 0.07 on average, while the KS tests reveal that such differences are significant at a confidence level of 99% at $10^{9.6} M_\odot \lesssim M_* \lesssim 10^{11.1} M_\odot$. These results are in good agreement with our finding based on the galaxy sizes.

Similar comparisons using the best-fit Sérsic index n extracted from the Meert et al. (2015) catalog are also examined. Due to the strong correlation between the

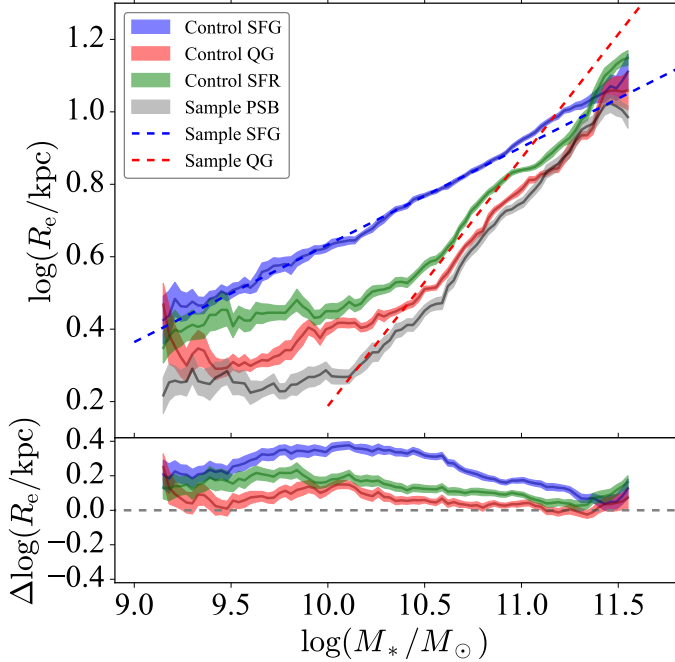


Figure 4. Size–mass relations for Sample PSB and three control samples. In the top panel, the blue, red, green, and black solid curves indicate the running medians of Samples Control SFG, Control QG, Control SFR (see text for more details), and PSB, respectively. The shadow regions around each median curve denote the corresponding $1\text{-}\sigma$ uncertainties. The blue and red dashed lines are the same as those in the left panel of Figure 3 (i.e., the best-fit relations for Samples SFG and QG, respectively). In the bottom panel, the differences in the running medians between Sample PSB and the three control samples are presented, together with the $1\text{-}\sigma$ uncertainties denoted as shadow regions.

concentrations and the Sérsic index n (Graham et al. 2005), we will not show the detailed results for n and just report that the index n of PSBs is larger than that of Control QG by 1.01 on average and the differences are significant at a confidence level of 99% at $10^{9.6} M_\odot \lesssim M_* \lesssim 10^{11.1} M_\odot$.

4. DISCUSSION

In this work, we investigate the size–mass relation for PSB galaxies in the local Universe and compare it with that of SFGs and QGs. Our results reveal a more compact morphology for PSBs compared to QGs with similar M_* for $M_* \lesssim 10^{11.0} M_\odot$, especially at $10^{9.5} M_\odot \lesssim M_* \lesssim 10^{10.5} M_\odot$ where the difference in galaxy size becomes larger and significant, indicating that similar morphological feature observed in higher-redshift PSBs (Almaini et al. 2017; Wu et al. 2018) still exists in the local Universe. In this section, we discuss possible implication of these results.

Table 1. Median sizes for Samples PSB, Control SFG, Control QG, and Control SFR.

Sample	$\log(M_*/M_\odot)$	$\log(R_e/\text{kpc})$	N
Sample PSB	9.0-9.3	0.22 ± 0.04	23
	9.3-9.6	0.27 ± 0.03	38
	9.6-9.9	0.23 ± 0.02	72
	9.9-10.2	0.27 ± 0.02	153
	10.2-10.5	0.39 ± 0.02	263
	10.5-10.8	0.53 ± 0.02	371
	10.8-11.1	0.73 ± 0.01	413
	11.1-11.4	0.89 ± 0.02	131
	11.4-11.7	0.99 ± 0.03	15
	Control SFG	9.0-9.3	0.43 ± 0.07
9.3-9.6		0.50 ± 0.02	113
9.6-9.9		0.58 ± 0.02	219
9.9-10.2		0.64 ± 0.01	460
10.2-10.5		0.73 ± 0.01	786
10.5-10.8		0.81 ± 0.01	1114
10.8-11.1		0.90 ± 0.01	1239
11.1-11.4		1.01 ± 0.01	390
11.4-11.7		1.11 ± 0.05	49
Control QG		9.0-9.3	0.47 ± 0.06
	9.3-9.6	0.29 ± 0.02	114
	9.6-9.9	0.33 ± 0.02	218
	9.9-10.2	0.42 ± 0.01	457
	10.2-10.5	0.45 ± 0.01	784
	10.5-10.8	0.58 ± 0.01	1116
	10.8-11.1	0.77 ± 0.01	1236
	11.1-11.4	0.90 ± 0.02	395
	11.4-11.7	1.06 ± 0.05	50
	Control SFR	9.0-9.3	0.35 ± 0.04
9.3-9.6		0.45 ± 0.05	110
9.6-9.9		0.45 ± 0.02	209
9.9-10.2		0.45 ± 0.02	426
10.2-10.5		0.53 ± 0.01	806
10.5-10.8		0.64 ± 0.01	1094
10.8-11.1		0.83 ± 0.01	1236
11.1-11.4		0.93 ± 0.02	396
11.4-11.7		1.15 ± 0.02	44

4.1. Different Evolution Pathways of PSBs

Previous works focused on the intermediate- or high-redshift (i.e., $z \gtrsim 0.5$) PSBs found that massive PSB galaxies (i.e., $M_* \gtrsim 10^{10} M_\odot$) have smaller or similar galaxy size in comparison with QGs at the same epoch (e.g., Belli et al. 2015; Yano et al. 2016; Almaini et al. 2017; Wu et al. 2018, 2020), supporting a fast quench-

Table 2. Differences in galaxy sizes and concentrations and the corresponding p -values from KS tests between PSBs and two control samples.

Sample	$\log(M_*/M_\odot)$	$\Delta \log(R_e/\text{kpc})$	p -value (R_e)	ΔC	p -value (C)
SF - PSB	9.0-9.3	0.21 ± 0.08	0.02	-0.41 ± 0.06	<0.01
	9.3-9.6	0.23 ± 0.04	<0.01	-0.37 ± 0.06	<0.01
	9.6-9.9	0.35 ± 0.03	<0.01	-0.40 ± 0.08	<0.01
	9.9-10.2	0.37 ± 0.02	<0.01	-0.44 ± 0.02	<0.01
	10.2-10.5	0.34 ± 0.02	<0.01	-0.56 ± 0.02	<0.01
	10.5-10.8	0.27 ± 0.02	<0.01	-0.59 ± 0.02	<0.01
	10.8-11.1	0.17 ± 0.01	<0.01	-0.61 ± 0.02	<0.01
	11.1-11.4	0.12 ± 0.02	<0.01	-0.52 ± 0.02	<0.01
QG - PSB	11.4-11.7	0.13 ± 0.06	0.04	-0.45 ± 0.09	<0.01
	9.0-9.3	0.25 ± 0.08	0.01	-0.29 ± 0.07	<0.01
	9.3-9.6	0.02 ± 0.04	0.46	-0.07 ± 0.06	0.12
	9.6-9.9	0.10 ± 0.03	<0.01	-0.11 ± 0.09	<0.01
	9.9-10.2	0.15 ± 0.02	<0.01	-0.07 ± 0.03	<0.01
	10.2-10.5	0.05 ± 0.02	<0.01	-0.09 ± 0.02	<0.01
	10.5-10.8	0.05 ± 0.02	0.02	-0.09 ± 0.02	<0.01
	10.8-11.1	0.04 ± 0.01	<0.01	-0.05 ± 0.02	<0.01
	11.1-11.4	0.01 ± 0.03	0.13	0.01 ± 0.02	0.07
	11.4-11.7	0.07 ± 0.06	0.05	0.06 ± 0.08	0.28

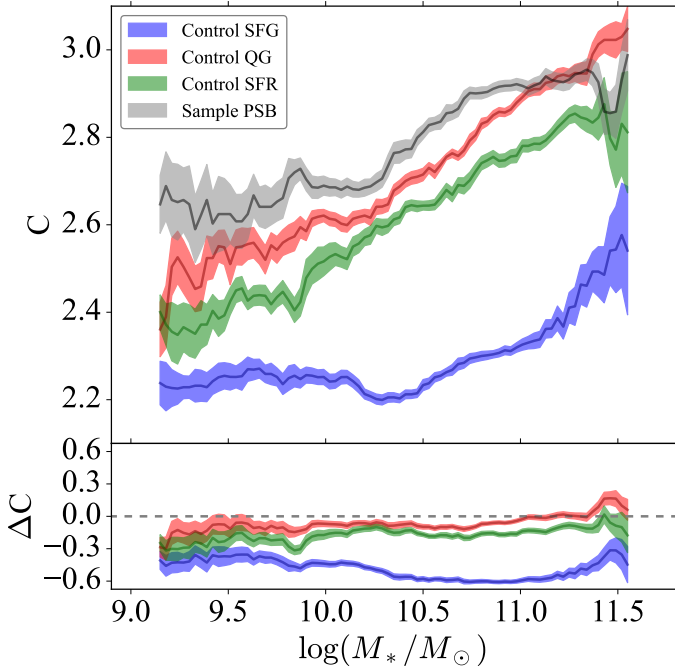


Figure 5. Comparisons of concentration $R_{90,r}/R_{50,r}$ between Sample PSB and three control samples. The symbols are the same as in Figure 4.

ing scenario in which galaxy structure is dramatically changed via a wet compaction before/during the quench-

ing of star formation (e.g., Dekel et al. 2009; Tacchella et al. 2016). However, few of these works reach the mass range of $M_* \lesssim 10^{10} M_\odot$.

On the other hand, observational studies about the local PSBs highlighted the diversity of this population and claimed various evolutionary pathways of PSBs including the fast quenching with significant structural changes and cyclic evolution without substantial morphological transformation (Pawlik et al. 2018). Based on the data products from cosmological simulations, Pawlik et al. (2019) further presented detailed descriptions of four typical examples of PSB galaxies, three of which are able to produce galaxy sizes as compact as QGs at a fixed M_* in their PSB phase. Since our results reveal that the morphology of PSBs resemble QGs rather than SFGs, we will attribute the dominated nature of our PSB sample to one of these compact PSBs in this section, while the last example that produces more disk-like, extended PSBs will be discussed in Section 4.2.

The three compact PSB prototypes represent three evolutionary pathways that all contain a distinct short-lived starburst and thus are able to exhibit observational spectral features of PSB galaxies, including a blue-to-red fast quenching, a blue-to-blue cycle (i.e., a SFG passes through a PSB phase after which the galaxy still maintains low level star formation), and a red-to-red rejuvenation (i.e., a QG enters a PSB phase and finally returns

to quiescent phase). The evident starbursts of the former two pathways are induced by a major merger, while the enhancement in SFR of the last one is due to a minor merger.

PSB galaxies in these channels are all able to have galaxy sizes comparable with those of QGs at a fixed M_* according to the similar concentrations between these two populations⁵ in simulations (Pawlik et al. 2019) and thus might have contributions to our PSB sample in observations. However, PSBs in the blue cycle are expected to have measurable H α emission due to their ongoing (low level) star formation activities, which are already rejected by our selection criterion of no-H α emission line described in Section 2.1. On the one hand, we also note that the time that the galaxy spent in the PSB phase of the red cycle is much smaller than that of the blue-to-red quenching (as shown in the Figure 3 of Pawlik et al. 2019), implying a very small possibility to observe a PSB in the red cycle (2% of PSBs identified in their simulations). On the other hand, simulations predicted little morphological change during the red cycle, in contrast to the smaller galaxy size we observed for PSBs compared to that of QGs. Meanwhile, in simulations the blue-to-red channel displays a decline in concentration index after the burst, indicating a more compact morphology at the beginning of the PSB phase. The gradual decrease of the concentration index during the PSB phase directly reflects a slight increase of the (light-weighted) galaxy size as the galaxy ages and fades down and finally reaches the quiescent phase with a size similar to typical QGs. Such picture drawn from the simulations is in good agreement with our observations.

Therefore, the blue cycle should have no contribution to our sample by selection, while the red cycle (if have) should be not the main mechanism for our PSBs. In term of the evolution channel of PSBs, we believe that the blue-to-red fast quenching following a short-lived starburst (might be induced by major merger) should be the dominated one.

4.2. Hint of Environmental Effect

Besides the three evolution channels with a short-lived burst of star formation, Pawlik et al. (2019) also claimed that about half of galaxies with PSB spectral features in their simulations have not underwent an evident merger-driven starburst event. This population is represented by the last example in Pawlik et al. (2019) for which

⁵ Both the blue-to-red quenching and the blue cycle undergo significant merger-induced morphological changes and the growth of a central spheroidal component, while the red cycle happens to a QG that already show spheroidal morphology.

the PSB features are caused by a rapid quenching of its continuous star formation after falling into a massive halo (galaxy cluster), i.e., an environmental effect.

Recent PSB studies about galaxy environment highlighted a nonnegligible effect of environment in the evolution of PSB galaxies (Poggianti et al. 2017; Paccagnella et al. 2019), especially for low- M_* PSB at $M_* \lesssim 10^{10} M_\odot$ (Socolovsky et al. 2018; Wilkinson et al. 2021). Based on photometrically selected PSBs at $0.5 < z < 1$, Socolovsky et al. (2018) found an excess of low- M_* PSB galaxies in clusters compared to less dense environments, while Wilkinson et al. (2021) reported that low- M_* PSBs prefer to reside in cluster-like environments. These studies suggested that fast quenching processes driven by dense environments might be one of the important mechanisms for low- M_* PSB in the local and intermediate-redshift Universe, as predicted by the simulations of Pawlik et al. (2019).

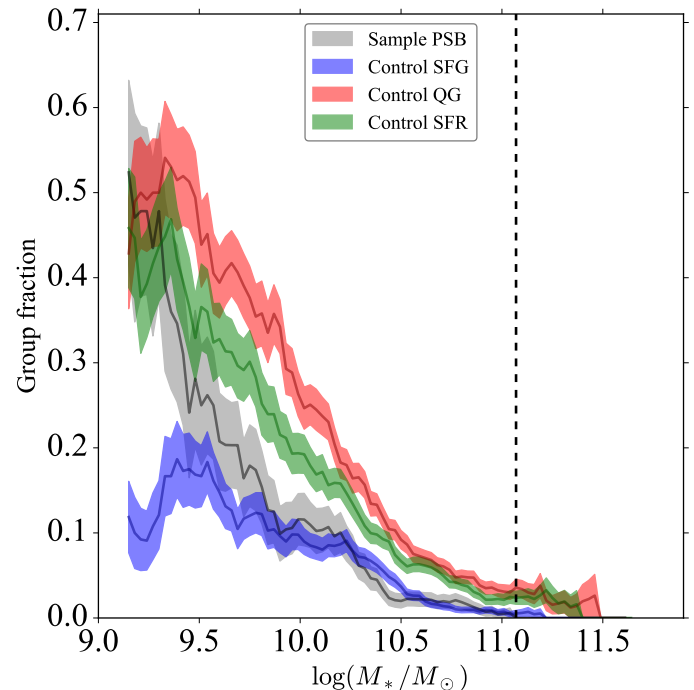


Figure 6. Group fractions as a function of stellar mass for Sample PSB and three control samples. The black dashed line marks the mass threshold of $M_* = 10^{11.07} M_\odot$ above which the fraction of the matched PSBs with the groups/clusters catalogs becomes lower than 50%. Symbols are the same as those in Figure 4.

To examine whether there is any environmental effect in our local PSB sample, we cross-match our samples with the catalogs of groups and clusters from Tempel et al. (2014) to identify PSBs resided in high density environments, and thus calculate the group frac-

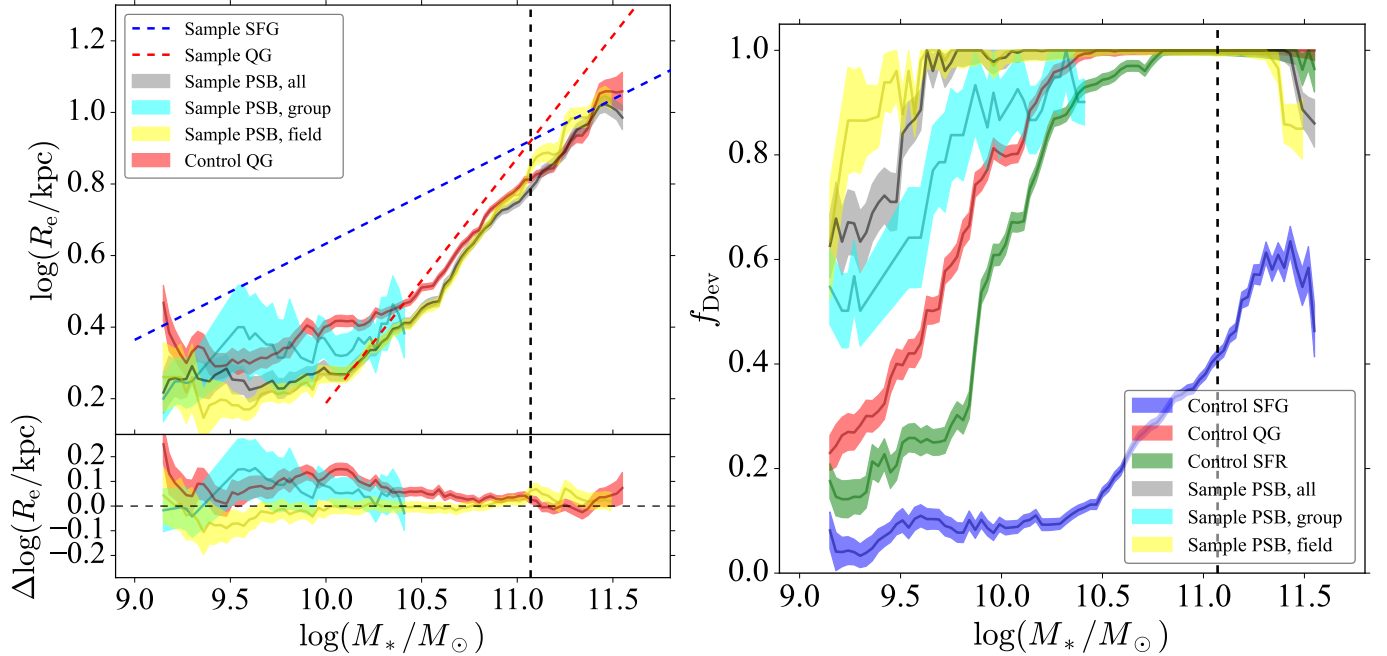


Figure 7. Size-mass relations (left) and f_{Dev} -mass relations for PSBs in different environments. The cyan (yellow) solid curves denote the median values of the corresponding parameters for PSBs in group (field), while the shadow regions are the 1- σ uncertainties. The black dashed line in each panel marks the mass threshold of $M_* = 10^{11.07} M_\odot$ above which the fraction of the matched PSBs with the groups/clusters catalogs becomes lower than 50%. Other symbols are the same as those in Figure 4.

tion (f_{group}) that describes the fraction of PSBs resided in a galaxy group within each M_* bin. Here, we define “galaxy groups” as those with number of members $N_{\text{member}} \geq 10$. Similar criteria are also adopted by other studies, e.g., Kim et al. (2020). We note that the final matched PSBs account for only 76% of Sample PSB due to two reasons: (1) a small fraction of sky sampled by our PSBs is not covered by the Tempel et al. (2014) catalogs, and (2) these catalogs only contain galaxies out to $z = 0.2$, while PSBs at $z > 0.2$ account for about 15% of our sample, which is also the most massive ones (i.e., $M_* \gtrsim 10^{11} M_\odot$). Figure 6 shows the group fraction as a function of M_* for Sample PSB, as well as for the three control samples for comparison. The black dashed line marks the mass threshold of $M_* = 10^{11.07} M_\odot$ above which the fraction of the matched PSBs with the groups/clusters catalogs becomes lower than 50%, and this highest- M_* regime will be ignored in the following discussion about the environmental effect.

Clearly, a general increase of the group fraction towards the low- M_* end is observed for all the samples. Sample Control SFR has an intermediate f_{group} between Samples Control SFG and QG, similar to their distributions in the M_* -SFR plane. Meanwhile, the f_{group} fraction of Sample PSB at $M_* \gtrsim 10^{10} M_\odot$ is small (i.e., $f_{\text{group}} \lesssim 10\%$), suggesting that most of massive PSBs are field galaxies and environment-related rapid quench-

ing processes (if have) have little or no contribution to PSBs at the high- M_* end. It is noteworthy that the local environment of these massive PSBs resembles that of Sample Control SFG rather than those of Samples Control SFR and QG, which is consistent with a picture in which a SFG undergoes a merger-induced starburst that followed by a rapid quenching and enters a PSB phase. At $M_* \lesssim 10^{10} M_\odot$, f_{group} of PSBs increases steeply towards the low- M_* end, while its differences from those of Samples Control SFR and QG become smaller. Local PSBs at $M_* \lesssim 10^{10} M_\odot$ are more clustered than their high- M_* analogues and SFGs with similar M_* . These trends are generally consistent with those reported in Wilkinson et al. (2021) for PSBs at $0.5 < z < 1.0$, implying a possible role of environment in the evolution of low- M_* PSBs.

To further explore how environments impact the galaxy sizes of PSBs, we divide Sample PSB into two subsamples according to their environments and our aforementioned group definition. Namely, we define PSBs resided in a galaxy group with $N_{\text{member}} \geq 10$ as group PSBs (i.e., Sample PSB, group), while the remaining isolated PSBs or those resided in a galaxy group with $N_{\text{member}} < 10$ are field PSBs (i.e., Sample PSB, field). The influence of adopting a different N_{member} criterion will be discussed in Section 4.3. In the left panel of Figure 7, we show the median mass-size relations for group

and field PSBs. The relation for field PSBs is almost the same as that of the whole Sample PSB except at the lowest- M_* end where field PSBs tend to be slightly smaller. The median mass-size relation shows a large dispersion, but it is still evident that the sizes of group PSBs tend to be larger compared to field PSBs. The R_e of group PSBs are $\sim 10\%$ larger on average than those of field PSBs at $M_* \lesssim 10^{10} M_\odot$. However, the KS test in the same M_* range only returns a p -value of 0.3, indicating that such differences are not significant enough, mainly due to the small number of group PSBs.

The environment-induced fast quenching process described in Pawlik et al. (2019) expects little morphological change and thus results in a disk-like PSB if the progenitor is also a star-forming disk before falling into the massive halo. As a simple check, we also use the flux fraction of the de Vaucouleurs component (f_{DeV}), which quantifies the flux ratio of the best-fit de Vaucouleurs component to the total flux when an exponential and a de Vaucouleurs models are combined to fit the galaxy image (see the online algorithm description⁶ for more details), in r -band extracted from the SDSS database to roughly evaluate the flux contribution of the central spheroidal component to the whole galaxy and whether a disk component is necessary. The $f_{\text{DeV}} = 1$ means that the galaxy is well described by a pure de Vaucouleurs profile, i.e., a compact spheroidal morphology without any disk component. The f_{DeV} as a function of M_* for group and field PSBs, as well as control samples, are presented in the right panel of Figure 7.

Again, the trends of f_{DeV} for Samples Control SFG, SFR, and QG are in good agreement with our expectation in which Sample Control SFR still exhibits its intermediate nature. As analogues of these control samples in the z - M_* or z - M_* -SFR parameter space, Sample PSB, however, shows a higher f_{DeV} (i.e., a much stronger spheroidal component), reinforcing our results demonstrated in Section 3. Disk-like components are only necessary for PSBs at $M_* \lesssim 10^{10} M_\odot$. Moreover, f_{DeV} of field PSBs is comparable to that of the whole PSB sample and larger than that of group PSBs, especially at the lowest- M_* end. A KS test between the f_{DeV} distributions of group and field PSBs at $M_* \lesssim 10^{10} M_\odot$ gives a p -value of 0.03, suggesting that the differences in f_{DeV} are statistically significant. In other words, group PSBs are more disk-like than field PSBs, implying that environments might (at least partly) account for the rapid quenching of PSBs in galaxy groups.

To summarize, environmental effects for local PSBs are observable only at $M_* \lesssim 10^{10} M_\odot$; group PSBs are observed to be slightly larger in galaxy size and more disk-like compared to field PSBs. These results are qualitatively consistent with the environment-driven fast quenching scenario described in Pawlik et al. (2019).

4.3. Influence of the Group Criterion

Our definition of “group” is based on the choice of number of members, which is set to $N_{\text{member}} \geq 10$ in this work. However, we also test smaller N_{member} and find that most of the results about the environments still stand up.

Specifically, we use a more relaxed galaxy group criterion $N_{\text{member}} \geq 5$ to define group PSBs and find that: (1) the overall trend and relative differences between f_{group} exhibited in Figure 6 are nearly unchanged although the absolute values are systematically higher, (2) the only difference of the size-mass relation for group/field PSBs is that more PSBs at $M_* \gtrsim 10^{10.5} M_\odot$ are classified as group PSBs and form a size-mass relation well consistent with that of field PSBs at $10^{10.5} M_\odot \lesssim M_* \lesssim 10^{11} M_\odot$, and (3) no substantial change is found for the f_{DeV} -mass relation.

4.4. Influence of Dust Effect on Sample Selection Criteria

Giving the aim of selecting galaxies with no ongoing star formation, as stated in Section 2.1, we adopt a criterion of $\text{EW}(\text{H}\alpha) < 3$ for $\text{H}\alpha$ emission lines. However, $\text{H}\alpha$ emission lines might suffer heavy dust attenuation, leading to the underestimation of the intrinsic fluxes and thus a risk that some SFGs are wrongly classified as PSBs. Given the low S/Ns of the observed emission lines for our PSBs, it is impossible to correct dust attenuation of $\text{EW}(\text{H}\alpha)$ via the widely used Balmer decrement method (i.e., the observe $\text{H}\alpha/\text{H}\beta$ flux ratio). Nevertheless, one can roughly estimate the unattenuated $\text{EW}(\text{H}\alpha)$ if the dust attenuation of the underlying stellar continuum is available. More specifically, the ratio between the intrinsic and observed $\text{EW}(\text{H}\alpha)$ can be written as

$$\begin{aligned} \log \left(\frac{\text{EW}(\text{H}\alpha)_{\text{int}}}{\text{EW}(\text{H}\alpha)_{\text{obs}}} \right) &= 0.4(A_{\text{H}\alpha, \text{gas}} - A_{\text{H}\alpha, \text{cont}}) \\ &= \frac{0.4k_{\text{H}\alpha}}{k_V}(A_{V, \text{gas}} - A_{V, \text{cont}}) \quad (1) \\ &= \frac{0.4k_{\text{H}\alpha}A_{V, \text{cont}}}{k_V} \left(\frac{1}{R_{\text{att}}} - 1 \right) \end{aligned}$$

in which $A_{\text{H}\alpha, \text{gas}}$ ($A_{V, \text{gas}}$) and $A_{\text{H}\alpha, \text{cont}}$ ($A_{V, \text{cont}}$) are the dust attenuation at the wavelength of $\text{H}\alpha$ (V band) for ionized gas and stellar continua, respectively; $k_{\text{H}\alpha}$ and

⁶ <https://www.sdss.org/dr12/algorithms/magnitudes/#cmodel>

k_V are defined via $k_\lambda = A_\lambda/E(B-V)$, namely the values of the assumed dust extinction/attenuation curve at the wavelengths of $H\alpha$ and V band (i.e., 5500 Å), respectively; $R_{\text{att}} = A_{V,\text{cont}}/A_{V,\text{gas}}$ is the dust attenuation ratio between ionized gas and stellar continua. Obviously, when dust attenuation of ionized gas is the same as that of stellar continua (i.e., $R_{\text{att}} = 1$), $\text{EW}(H\alpha)_{\text{int}} = \text{EW}(H\alpha)_{\text{obs}}$, i.e., correction for dust is unnecessary. In this case, our $\text{EW}(H\alpha)$ criterion is unaffected by dust. However, heavier dust attenuation for ionized gas compared to stellar light (i.e., $R_{\text{att}} < 1$) is reported by observations of SFGs (e.g., Calzetti 1997), while R_{att} is also found to strongly depend on other physical properties, such as M_* (Zahid et al. 2017; Koyama et al. 2019; Lin & Kong 2020).

To roughly evaluate the influence of this effect, we use Equation (1) to estimate the dust correction for $\text{EW}(H\alpha)$. $A_{V,\text{cont}}$ can be derived via $\tau_{V,\text{cont}} = A_{V,\text{cont}}/1.086$ where $\tau_{V,\text{cont}}$ is the V band optical depth extracted from the MPA-JHU catalog and derived from the best-fit model of photometry fitting. The M_*-R_{att} relation of $R_{\text{att}} = 3.460 - 0.277 \times \log(M_*/M_\odot)$ for local SFGs (Lin & Kong 2020) is adopted to obtain R_{att} for each galaxy. An extinction curve of Cardelli et al. (1989) and $R_V = 3.1$ are assumed. After $\text{EW}(H\alpha)_{\text{int}}$ is obtained, we use this dust corrected $\text{EW}(H\alpha)$ to redo the sample selection and find that only 388 (26.2%) galaxies are removed from the original Sample PSB. After carefully remaking figures and tables, we finally find that our main results are nearly unchanged given this dust corrected PSB sample.

Giving the difficulty of correction for dust and the possible large uncertainties of attenuation introduced by this correction, such dust effect is not accounted for in most of previous spectroscopically selected PSB studies (e.g., Zahid et al. 2016; Chen et al. 2019). In order to be in consonance with previous works, we therefore do not correct this effect in our analyses and just represent a short discussion on its influence here.

4.5. Other Issues Related to Galaxy Size Measurements

In this section, we will discuss three issues related to the galaxy size measurements, i.e., the PSF effects, the sampled rest-frame wavelengths, and the systematic uncertainties in R_e estimation.

As described in Section 2.2 galaxy size measurements used in this work are R_e derived from the single Sérsic fits extracted from the Meert et al. (2015) catalog, which are carried out by GALFIT (Peng et al. 2002). Our results reveal that PSB galaxies tend to have extremely small sizes, specially at the low- M_* end. However, the existence of a large PSF will prevent us from obtaining

reliable size measurements for very compact sources. In GALFIT, the effect of PSF is accounted for during the model fitting. The code uses convolution technique to account for this effect, namely convolves the model image (e.g., a Sérsic profile) with the PSF before comparing the result with the observed image (Peng et al. 2002). Meert et al. (2015) presented a discussion on how the PSF affects size measurement of bulge (i.e., the central compact component of galaxies) and claimed that bulge sizes smaller than 80% of the half-width at half-maximum (HWHM) of the PSF can be overestimated (Gadotti 2008). Such bias might also exist in the single Sérsic fits for compact galaxies, e.g., our PSB sample.

Given that the HWHM of the PSF for SDSS is about 0.7'' in the r -band⁷, our further check finds that only 5.2% of our PSBs have R_e smaller than $0.8 \times \text{HWHM}$. This small portion of the PSB sample is concentrated between $10^{10} M_\odot < M_* < 10^{11} M_\odot$ and could not bias the trend at the high- or low- M_* end where the number of PSBs is small. Therefore, the potential PSF effect is too small to have significant influence on our results.

Enabling a direct comparison of size-mass relation with previous PSB studies (e.g., Yano et al. 2016; Almaini et al. 2017; Wu et al. 2018, 2020) requires consistent size measurements with these works in terms of not only the derivation method but also the sampled rest-frame wavelengths since galaxy size might vary with wavelengths. In this work, the former condition is naturally met by design (see Section 2.2). The latter one is also generally satisfied, although misplacement of wavelengths still exists but is proved to have no influence on our main results as discussed below.

The Sérsic R_e we adopted in this work is based on the SDSS r -band image, for which the central wavelength corresponds to a rest-frame wavelength of ~ 5500 Å given a median redshift of $z = 0.13$ and generally covers the rest-frame g - and r - bands (i.e., $\sim 4600 - 6200$ Å) given the redshift range of our PSB sample. Due to the different redshift ranges and images used, the rest-frame wavelengths sampled by previous studies span a large range from ~ 4100 Å (g -band; e.g., Wu et al. 2018, 2020) to ~ 8400 Å (i -band; e.g., Belli et al. 2015). Although all of these works share part of the sampled rest-frame wavelength coverage with our PSB sample, we still note that some galaxies in these samples might move out of the coverage of our sample. We thus further check the main results by using the Sérsic R_e derived based on the SDSS g - and i -band images, which are also provided by the Meert et al. (2015) catalog, and find that these

⁷ <https://www.sdss.org/dr12/scope/>

results are unchanged when g - or i -band Sérsic R_e are considered. In other words, the observed differences in galaxy sizes between PSBs and QGs can be found from g -band to i -band, thus our comparison with previous studies are still reasonable.

Finally, we discuss the systematic uncertainties arising from adopting a single Sérsic profile to describe the light profiles of PSB galaxies. As demonstrated in Meert et al. (2013), the single Sérsic fit of PyMorph is able to give an unbiased estimation of R_e with a small scatter ($\sim 5\%$) for a galaxy with a Sérsic profile, however, applying the same fit to a galaxy with a two-component Sérsic + Exponential profile might result in an overestimation of $\sim 5\%$ in R_e at the faint end.

We compute the fraction of galaxies that better described by a single Sérsic model rather than a Sérsic + Exponential model for PSBs and all control samples. This fraction of PSBs is found to be comparable with that of Sample Control QG at $M_* \gtrsim 10^{10.5} M_\odot$, but tends to become smaller up to 13% at the low- M_* end. When we perform a galaxy size comparison between PSBs and QGs, the systematic overestimation of R_e of PSBs might be more serious compared to that of QGs, possibly resulting in an underestimation of the differences in R_e at the low- M_* end. Therefore, our main results should be unchanged even when the systematic uncertainties in R_e estimation is considered.

5. SUMMARY

We present a study of the size-mass relation for local PSB galaxies sample selected from the SDSS DR8. We compile a sample of 1,479 PSB galaxies at $0.012 < z < 0.324$. Control samples are constructed to compare PSBs with SFGs and QGs and discuss the possible evolutionary pathways of our PSB galaxies. Our main conclusions are as follows:

1. Due to the limited magnitude of the SDSS spectra, our spectrally selected PSB sample is biased towards the massive end of local PSBs, although less massive PSBs at $M_* \lesssim 10^{10} M_\odot$ are expected to dominate this population based on studies of photometrically selected PSBs.
2. Whether a z - M_* control sample is constructed or not, the sizes of PSBs are smaller than those of QGs in the vast majority of M_* bins we explore, such differences become larger towards the low- M_* end. The z - M_* -SFR control sample further reinforces the result of an extreme compact morphology for local PSBs. Examination using an independent measurement of concentration or the Sérsic index also supports these results.
3. By comparing with predictions of possible PSB evolutionary pathways from cosmological simulations, we demonstrate that the SFG-to-QG fast quenching following a short-lived starburst event (might be induced by major merger) should be the dominated pathway of our PSB sample.
4. Local PSBs at $M_* \lesssim 10^{10} M_\odot$ are more clustered than more massive PSBs. Group PSBs are observed to be slightly larger in galaxy size and more disk-like compared to field PSBs, hinting an environment-driven fast quenching pathway for group PSBs, especially at $M_* \lesssim 10^{10} M_\odot$.

The evolutionary pathway of massive PSB galaxies is clearer compared to PSBs at $M_* \lesssim 10^{10} M_\odot$. Although our observations qualitatively support the environment-driven fast quenching scenario described in Pawlik et al. (2019), stronger (quantitative) conclusion about the environmental effect cannot be drawn due to the small number of low- M_* PSBs in our sample. Observations of a large sample of low- M_* PSBs are needed to clarify the role of environments in the evolution of PSB galaxies.

ACKNOWLEDGEMENTS

We would like to thank the referee for many helpful comments and suggestions, which greatly improve the paper. This work is supported by the Strategic Priority Research Program of Chinese Academy of Sciences (No. XDB 41000000), the National Key R&D Program of China (2017YFA0402600, 2017YFA0402702), the NSFC grant (Nos. 11973038 and 11973039), and the Chinese Space Station Telescope (CSST) Project. HXZ also thanks a support from the CAS Pioneer Hundred Talents Program. Z.S.L acknowledges the support from China Postdoctoral Science Foundation (2021M700137).

This research has made use of the SIMBAD database, operated at CDS, Strasbourg, France. All plots in this paper were built with the MATPLOTLIB package for PYTHON (Hunter 2007).

Funding for SDSS-III has been provided by the Alfred P. Sloan Foundation, the Participating Institutions, the National Science Foundation, and the U.S. Department of Energy Office of Science. The SDSS-III web site is <http://www.sdss3.org/>.

SDSS-III is managed by the Astrophysical Research Consortium for the Participating Institutions of the SDSS-III Collaboration including the University of Arizona, the Brazilian Participation Group, Brookhaven National Laboratory, Carnegie Mellon University, University of Florida, the French Participation Group, the German Participation Group, Harvard University, the Instituto de Astrofísica de Canarias, the Michigan

State/Notre Dame/JINA Participation Group, Johns Hopkins University, Lawrence Berkeley National Laboratory, Max Planck Institute for Astrophysics, Max Planck Institute for Extraterrestrial Physics, New Mexico State University, New York University, Ohio State

University, Pennsylvania State University, University of Portsmouth, Princeton University, the Spanish Participation Group, University of Tokyo, University of Utah, Vanderbilt University, University of Virginia, University of Washington, and Yale University.

REFERENCES

- Aihara, H., Allende Prieto, C., An, D., et al. 2011, *The Astrophysical Journal Supplement Series*, 193, 29, doi: [10.1088/0067-0049/193/2/29](https://doi.org/10.1088/0067-0049/193/2/29)
- Almaini, O., Wild, V., Maltby, D. T., et al. 2017, *Monthly Notices of the Royal Astronomical Society*, 472, 1401, doi: [10.1093/mnras/stx1957](https://doi.org/10.1093/mnras/stx1957)
- Baldry, I. K., Glazebrook, K., Brinkmann, J., et al. 2004, *The Astrophysical Journal*, 600, 681, doi: [10.1086/380092](https://doi.org/10.1086/380092)
- Bell, E. F., McIntosh, D. H., Katz, N., & Weinberg, M. D. 2003, *The Astrophysical Journal Supplement Series*, 149, 289, doi: [10.1086/378847](https://doi.org/10.1086/378847)
- Belli, S., Newman, A. B., & Ellis, R. S. 2015, *The Astrophysical Journal*, 799, 206, doi: [10.1088/0004-637X/799/2/206](https://doi.org/10.1088/0004-637X/799/2/206)
- Bertin, E., & Arnouts, S. 1996, *Astronomy and Astrophysics Supplement Series*, 117, 393, doi: [10.1051/aas:1996164](https://doi.org/10.1051/aas:1996164)
- Brinchmann, J., Charlot, S., White, S. D. M., et al. 2004, *Monthly Notices of the Royal Astronomical Society*, 351, 1151, doi: [10.1111/j.1365-2966.2004.07881.x](https://doi.org/10.1111/j.1365-2966.2004.07881.x)
- Bruzual, G., & Charlot, S. 2003, *MNRAS*, 344, 1000, doi: [10.1046/j.1365-8711.2003.06897.x](https://doi.org/10.1046/j.1365-8711.2003.06897.x)
- Calzetti, D. 1997, in *American Institute of Physics Conference Series*, Vol. 408, *The ultraviolet universe at low and High redshift*, ed. W. H. Waller, 403–412, doi: [10.1063/1.53764](https://doi.org/10.1063/1.53764)
- Cardelli, J. A., Clayton, G. C., & Mathis, J. S. 1989, *ApJ*, 345, 245, doi: [10.1086/167900](https://doi.org/10.1086/167900)
- Charlot, S., & Fall, S. M. 2000, *ApJ*, 539, 718, doi: [10.1086/309250](https://doi.org/10.1086/309250)
- Chen, Y.-M., Shi, Y., Wild, V., et al. 2019, *Monthly Notices of the Royal Astronomical Society*, 489, 5709, doi: [10.1093/mnras/stz2494](https://doi.org/10.1093/mnras/stz2494)
- Dekel, A., Birnboim, Y., Engel, G., et al. 2009, *Nature*, 457, 451, doi: [10.1038/nature07648](https://doi.org/10.1038/nature07648)
- D'Eugenio, F., van der Wel, A., Wu, P.-F., et al. 2020, *Monthly Notices of the Royal Astronomical Society*, doi: [10.1093/mnras/staa1937](https://doi.org/10.1093/mnras/staa1937)
- Dressler, A., & Gunn, J. E. 1983, *The Astrophysical Journal*, 270, 7, doi: [10.1086/161093](https://doi.org/10.1086/161093)
- Gadotti, D. A. 2008, *MNRAS*, 384, 420, doi: [10.1111/j.1365-2966.2007.12723.x](https://doi.org/10.1111/j.1365-2966.2007.12723.x)
- Goto, T. 2005, *Monthly Notices of the Royal Astronomical Society*, 357, 937, doi: [10.1111/j.1365-2966.2005.08701.x](https://doi.org/10.1111/j.1365-2966.2005.08701.x)
- . 2007, *Monthly Notices of the Royal Astronomical Society*, 381, 187, doi: [10.1111/j.1365-2966.2007.12227.x](https://doi.org/10.1111/j.1365-2966.2007.12227.x)
- Graham, A. W., Driver, S. P., Petrosian, V., et al. 2005, *The Astronomical Journal*, 130, 1535, doi: [10.1086/444475](https://doi.org/10.1086/444475)
- Greene, O. A., Anderson, M. R., Marinelli, M., et al. 2021, *The Astrophysical Journal*, 910, 162, doi: [10.3847/1538-4357/abe4d1](https://doi.org/10.3847/1538-4357/abe4d1)
- Gu, Y., Fang, G., Yuan, Q., Cai, Z., & Wang, T. 2018, *The Astrophysical Journal*, 855, 10, doi: [10.3847/1538-4357/aaad0b](https://doi.org/10.3847/1538-4357/aaad0b)
- Hopkins, P. F., Cox, T. J., Hernquist, L., et al. 2013, *Monthly Notices of the Royal Astronomical Society*, 430, 1901, doi: [10.1093/mnras/stt017](https://doi.org/10.1093/mnras/stt017)
- Hunter, J. D. 2007, *Computing in Science and Engineering*, 9, 90, doi: [10.1109/MCSE.2007.55](https://doi.org/10.1109/MCSE.2007.55)
- Kauffmann, G., Heckman, T. M., White, S. D. M., et al. 2003, *Monthly Notices of the Royal Astronomical Society*, 341, 33, doi: [10.1046/j.1365-8711.2003.06291.x](https://doi.org/10.1046/j.1365-8711.2003.06291.x)
- Kawinwanichakij, L., Silverman, J. D., Ding, X., et al. 2021, *The Astrophysical Journal*, 921, 38, doi: [10.3847/1538-4357/ac1f21](https://doi.org/10.3847/1538-4357/ac1f21)
- Kim, S., Jeong, H., Rey, S.-C., et al. 2020, *The Astrophysical Journal*, 903, 65, doi: [10.3847/1538-4357/abaef5](https://doi.org/10.3847/1538-4357/abaef5)
- Koyama, Y., Shimakawa, R., Yamamura, I., Kodama, T., & Hayashi, M. 2019, *PASJ*, 71, 8, doi: [10.1093/pasj/psy113](https://doi.org/10.1093/pasj/psy113)
- Kroupa, P. 2001, *Monthly Notices of the Royal Astronomical Society*, 322, 231, doi: [10.1046/j.1365-8711.2001.04022.x](https://doi.org/10.1046/j.1365-8711.2001.04022.x)
- Lin, L., Ellison, S. L., Pan, H.-A., et al. 2022, *The Astrophysical Journal*, 926, 175, doi: [10.3847/1538-4357/ac4ccc](https://doi.org/10.3847/1538-4357/ac4ccc)
- Lin, Z., & Kong, X. 2020, *ApJ*, 888, 88, doi: [10.3847/1538-4357/ab5f0e](https://doi.org/10.3847/1538-4357/ab5f0e)
- Maltby, D. T., Almaini, O., Wild, V., et al. 2018, *Monthly Notices of the Royal Astronomical Society*, 480, 381, doi: [10.1093/mnras/sty1794](https://doi.org/10.1093/mnras/sty1794)

- Martin, D. C., Wyder, T. K., Schiminovich, D., et al. 2007, *The Astrophysical Journal Supplement Series*, 173, 342, doi: [10.1086/516639](https://doi.org/10.1086/516639)
- Meert, A., Vikram, V., & Bernardi, M. 2013, *MNRAS*, 433, 1344, doi: [10.1093/mnras/stt822](https://doi.org/10.1093/mnras/stt822)
- Meert, A., Vikram, V., & Bernardi, M. 2015, *Monthly Notices of the Royal Astronomical Society*, 446, 3943, doi: [10.1093/mnras/stu2333](https://doi.org/10.1093/mnras/stu2333)
- . 2016, *Monthly Notices of the Royal Astronomical Society*, 455, 2440, doi: [10.1093/mnras/stv2475](https://doi.org/10.1093/mnras/stv2475)
- Mosleh, M., Williams, R. J., & Franx, M. 2013, *The Astrophysical Journal*, 777, 117, doi: [10.1088/0004-637X/777/2/117](https://doi.org/10.1088/0004-637X/777/2/117)
- Mowla, L. A., van Dokkum, P., Brammer, G. B., et al. 2019, *The Astrophysical Journal*, 880, 57, doi: [10.3847/1538-4357/ab290a](https://doi.org/10.3847/1538-4357/ab290a)
- Newman, A. B., Ellis, R. S., Bundy, K., & Treu, T. 2012, *The Astrophysical Journal*, 746, 162, doi: [10.1088/0004-637X/746/2/162](https://doi.org/10.1088/0004-637X/746/2/162)
- Paccagnella, A., Vulcani, B., Poggianti, B. M., et al. 2019, *Monthly Notices of the Royal Astronomical Society*, 482, 881, doi: [10.1093/mnras/sty2728](https://doi.org/10.1093/mnras/sty2728)
- Pawlik, M. M., McAlpine, S., Trayford, J. W., et al. 2019, *Nature Astronomy*, 3, 440, doi: [10.1038/s41550-019-0725-z](https://doi.org/10.1038/s41550-019-0725-z)
- Pawlik, M. M., Taj Aldeen, L., Wild, V., et al. 2018, *Monthly Notices of the Royal Astronomical Society*, 477, 1708, doi: [10.1093/mnras/sty589](https://doi.org/10.1093/mnras/sty589)
- Peng, C. Y., Ho, L. C., Impey, C. D., & Rix, H.-W. 2002, *The Astronomical Journal*, 124, 266, doi: [10.1086/340952](https://doi.org/10.1086/340952)
- Poggianti, B. M., Smail, I., Dressler, A., et al. 1999, *The Astrophysical Journal*, 518, 576, doi: [10.1086/307322](https://doi.org/10.1086/307322)
- Poggianti, B. M., Moretti, A., Gullieuszik, M., et al. 2017, *The Astrophysical Journal*, 844, 48, doi: [10.3847/1538-4357/aa78ed](https://doi.org/10.3847/1538-4357/aa78ed)
- Roy, N., Napolitano, N. R., La Barbera, F., et al. 2018, *Monthly Notices of the Royal Astronomical Society*, 480, 1057, doi: [10.1093/mnras/sty1917](https://doi.org/10.1093/mnras/sty1917)
- Salim, S. 2014, *Serbian Astronomical Journal*, 189, 1, doi: [10.2298/SAJ1489001S](https://doi.org/10.2298/SAJ1489001S)
- Salim, S., Rich, R. M., Charlot, S., et al. 2007, *The Astrophysical Journal Supplement Series*, 173, 267, doi: [10.1086/519218](https://doi.org/10.1086/519218)
- Schawinski, K., Urry, C. M., Simmons, B. D., et al. 2014, *Monthly Notices of the Royal Astronomical Society*, 440, 889, doi: [10.1093/mnras/stu327](https://doi.org/10.1093/mnras/stu327)
- Schiminovich, D., Wyder, T. K., Martin, D. C., et al. 2007, *The Astrophysical Journal Supplement Series*, 173, 315, doi: [10.1086/524659](https://doi.org/10.1086/524659)
- Shen, S., Mo, H. J., White, S. D. M., et al. 2003, *Monthly Notices of the Royal Astronomical Society*, 343, 978, doi: [10.1046/j.1365-8711.2003.06740.x](https://doi.org/10.1046/j.1365-8711.2003.06740.x)
- Shibuya, T., Ouchi, M., & Harikane, Y. 2015, *The Astrophysical Journal Supplement Series*, 219, 15, doi: [10.1088/0067-0049/219/2/15](https://doi.org/10.1088/0067-0049/219/2/15)
- Socolovsky, M., Almaini, O., Hatch, N. A., et al. 2018, *Monthly Notices of the Royal Astronomical Society*, 476, 1242, doi: [10.1093/mnras/sty312](https://doi.org/10.1093/mnras/sty312)
- Strauss, M. A., Weinberg, D. H., Lupton, R. H., et al. 2002, *The Astronomical Journal*, 124, 1810, doi: [10.1086/342343](https://doi.org/10.1086/342343)
- Suess, K. A., Kriek, M., Price, S. H., & Barro, G. 2021, *The Astrophysical Journal*, 915, 87, doi: [10.3847/1538-4357/abf1e4](https://doi.org/10.3847/1538-4357/abf1e4)
- Tacchella, S., Dekel, A., Carollo, C. M., et al. 2016, *Monthly Notices of the Royal Astronomical Society*, 458, 242, doi: [10.1093/mnras/stw303](https://doi.org/10.1093/mnras/stw303)
- Tempel, E., Tamm, A., Gramann, M., et al. 2014, *Astronomy and Astrophysics*, 566, A1, doi: [10.1051/0004-6361/201423585](https://doi.org/10.1051/0004-6361/201423585)
- van der Wel, A., Franx, M., van Dokkum, P. G., et al. 2014, *The Astrophysical Journal*, 788, 28, doi: [10.1088/0004-637X/788/1/28](https://doi.org/10.1088/0004-637X/788/1/28)
- Vikram, V., Wadadekar, Y., Kembhavi, A. K., & Vijayagovindan, G. V. 2010, *Monthly Notices of the Royal Astronomical Society*, 409, 1379, doi: [10.1111/j.1365-2966.2010.17426.x](https://doi.org/10.1111/j.1365-2966.2010.17426.x)
- Wellons, S., Torrey, P., Ma, C.-P., et al. 2015, *Monthly Notices of the Royal Astronomical Society*, 449, 361, doi: [10.1093/mnras/stv303](https://doi.org/10.1093/mnras/stv303)
- Wenger, M., Ochsenein, F., Egret, D., et al. 2000, *Astronomy and Astrophysics Supplement Series*, 143, 9, doi: [10.1051/aas:2000332](https://doi.org/10.1051/aas:2000332)
- Whitaker, K. E., Kriek, M., van Dokkum, P. G., et al. 2012, *The Astrophysical Journal*, 745, 179, doi: [10.1088/0004-637X/745/2/179](https://doi.org/10.1088/0004-637X/745/2/179)
- Wild, V., Almaini, O., Dunlop, J., et al. 2016, *Monthly Notices of the Royal Astronomical Society*, 463, 832, doi: [10.1093/mnras/stw1996](https://doi.org/10.1093/mnras/stw1996)
- Wild, V., Kauffmann, G., Heckman, T., et al. 2007, *Monthly Notices of the Royal Astronomical Society*, 381, 543, doi: [10.1111/j.1365-2966.2007.12256.x](https://doi.org/10.1111/j.1365-2966.2007.12256.x)
- Wild, V., Walcher, C. J., Johansson, P. H., et al. 2009, *Monthly Notices of the Royal Astronomical Society*, 395, 144, doi: [10.1111/j.1365-2966.2009.14537.x](https://doi.org/10.1111/j.1365-2966.2009.14537.x)
- Wilkinson, A., Almaini, O., Wild, V., et al. 2021, *Monthly Notices of the Royal Astronomical Society*, 504, 4533, doi: [10.1093/mnras/stab965](https://doi.org/10.1093/mnras/stab965)

- Williams, R. J., Quadri, R. F., Franx, M., et al. 2010, *The Astrophysical Journal*, 713, 738, doi: [10.1088/0004-637X/713/2/738](https://doi.org/10.1088/0004-637X/713/2/738)
- Wong, O. I., Schawinski, K., Kaviraj, S., et al. 2012, *Monthly Notices of the Royal Astronomical Society*, 420, 1684, doi: [10.1111/j.1365-2966.2011.20159.x](https://doi.org/10.1111/j.1365-2966.2011.20159.x)
- Woo, J., Dekel, A., Faber, S. M., et al. 2013, *Monthly Notices of the Royal Astronomical Society*, 428, 3306, doi: [10.1093/mnras/sts274](https://doi.org/10.1093/mnras/sts274)
- Wu, P.-F., van der Wel, A., Bezanson, R., et al. 2018, *The Astrophysical Journal*, 868, 37, doi: [10.3847/1538-4357/aae822](https://doi.org/10.3847/1538-4357/aae822)
- . 2020, *The Astrophysical Journal*, 888, 77, doi: [10.3847/1538-4357/ab5fd9](https://doi.org/10.3847/1538-4357/ab5fd9)
- Wyder, T. K., Martin, D. C., Schiminovich, D., et al. 2007, *The Astrophysical Journal Supplement Series*, 173, 293, doi: [10.1086/521402](https://doi.org/10.1086/521402)
- Yan, R., Newman, J. A., Faber, S. M., et al. 2006, *The Astrophysical Journal*, 648, 281, doi: [10.1086/505629](https://doi.org/10.1086/505629)
- Yano, M., Kriek, M., van der Wel, A., & Whitaker, K. E. 2016, *The Astrophysical Journal Letters*, 817, L21, doi: [10.3847/2041-8205/817/2/L21](https://doi.org/10.3847/2041-8205/817/2/L21)
- Yesuf, H. M., Faber, S. M., Trump, J. R., et al. 2014, *The Astrophysical Journal*, 792, 84, doi: [10.1088/0004-637X/792/2/84](https://doi.org/10.1088/0004-637X/792/2/84)
- Zahid, H. J., Baeza Hochmuth, N., Geller, M. J., et al. 2016, *ApJ*, 831, 146, doi: [10.3847/0004-637X/831/2/146](https://doi.org/10.3847/0004-637X/831/2/146)
- Zahid, H. J., Kudritzki, R.-P., Conroy, C., Andrews, B., & Ho, I. T. 2017, *ApJ*, 847, 18, doi: [10.3847/1538-4357/aa88ae](https://doi.org/10.3847/1538-4357/aa88ae)